D. G. Gregory-Smith
School of Engineering and Applied Science,
University of Durham,
Durham, DH1 3LE, United Kingdom

C. P. Graves
Gilbert Gilkes & Gordon Ltd.,
Kendal, Cumbria, LA9 7BZ, United Kingdom

J. A. Walsh
Logica Space and Defence Systems Ltd.,
London, W1A 4SE, United Kingdom

Growth of Secondary Losses and Vorticity in an Axial Turbine Cascade

The growth of losses, secondary kinetic energy, and streamwise vorticity have been studied in a high turning rotor cascade. Negative vorticity associated with the passage vortex agreed well with predictions of classical secondary flow theory in the early part of the blade passage. However, toward the exit, the distortion of the flow by the secondary velocities rendered the predictions inaccurate. Areas of positive vorticity were associated with the feeding of loss into the bulk flow and have been related to separation lines observed by surface flow visualization.

Introduction

The term "secondary flows" is usually used to describe the transverse velocities that are generated when a shear flow is turned. In a turbine, secondary flows are generated from the endwall boundary layers on the casing or hub of the machine, and because the turning is great, the secondary flows may be large. The practical significance is the change in deflection through a blade row and the generation of secondary losses, which may amount to half the total losses through the machine.

In terms of classical secondary flow theory, e.g., Squire and Winter (1951), Hawthorne (1951, 1967), Came and Marsh (1974), and Horlock and Lakshminarayana (1973), the turning of the vorticity vector through a blade row gives a component of vorticity in the streamwise direction, thus generating transverse velocities. In the secondary flow approximation (Hawthorne, 1967), the vortex filaments are convected by a primary flow, which is undisturbed by the secondary velocities. Thus the Bernoulli surfaces (surfaces of constant total pressure) remain parallel to the endwall throughout the blade row, and are not distorted by the secondary flow. Downstream of the blade row there are three contributions to the streamwise vorticity. Firstly, there is the distributed secondary vorticity, which generates secondary velocities in the blade passage. Then there are two shed vorticities that appear in the blade wake, the trailing filament vorticity that arises from the stretching of the vortex lines as they pass around the blades, and the trailing shed vorticity that arises from the spanwise variation in circulation around the blades.

This cascade volume view (i.e., looking at only the inlet and outlet flows of the blade row) does not consider the complex details of the flow within the blade passage. These details have to be understood if an understanding of the loss generating mechanisms is to be gained. In recent years a lot of effort has been made to look at the details of endwall flows in axial turbines. These have been comprehensively reviewed by Sieverding (1985). Most of the work has been carried out using pressure probes to gain quantitative data for flow angles and total pressure losses, and using flow visualization to give qualitative information on separation lines and the formation of vortices. However little appears in the published literature on the quantitative development of streamwise vorticity that can be linked with the ideas of classical secondary flow theory. The reason for this may be the difficulty in differentiating experimental data and the fairly high resolution of data points required to get acceptable accuracy.

A program at Durham University is studying the details of secondary flows in a high turning turbine rotor blade. Some results for the flow development have been reported by Gregory-Smith and Graves (1983). This paper presents data on the development of streamwise vorticity through the blade passage and aims to relate this to the generation of loss caused by the secondary flows.

Table 1 Cascade design data

Flow inlet angle	42.75 deg
Blade exit angle	−67.5 deg
Blade chord	216 mm
Axial chord	175 mm
Span	457 mm
Pitch	191 mm
Aspect ratio	2.1
Reynolds number (blade chord and exit velocity)	5×10^5

Table 2 Inlet boundary layer data

Boundary layer type	Natural	Thick	Thin
Displacement thickness	12.1 mm	27.9 mm	9.7 mm
Momentum thickness	9.9 mm	19.7 mm	7.6 mm
Estimated 99 percent thickness	102 mm	150 mm	82 mm
Total pressure loss coefficient	0.084	0.175	0.054

Apparatus

The turbine rotor blades were set in a linear cascade and operated at incompressible flow velocities. The cascade is

Contributed by the Gas Turbine Division of THE AMERICAN SOCIETY OF MECHANICAL ENGINEERS and presented at the 32nd International Gas Turbine Conference and Exhibit, Anaheim, California, May 31–June 4, 1987. Manuscript received at ASME Headquarters February 10, 1987. Paper No. 87-GT-114.

described in detail by Graves (1985), and Table 1 gives the main geometric parameters.

The cascade was traversed using a five-hole cobra-type probe at ten axial positions as shown in Fig. 1. In addition flow visualization was carried out on the endwall and blade surfaces using a fluorescent powder dye and light oil mixture. The above measurements were made with a "natural" inlet boundary layer. Traverses at the upstream and downstream positions were also carried out for a "thickened" and "thinned" inlet boundary layer. The features of the inlet boundary layers are summarized in Table 2.

The loss coefficient is defined with respect to the *inlet* dynamic pressure.

The measurements were recorded using a data acquisition system controlled by a microcomputer and the recorded data were transferred to a mainframe computer for analysis and plotting. The angles, velocity vectors, and pressures were obtained directly from the calibration of the five-hole probe. However the derivation of vorticity is not straightforward and is described below.

Derivation of Streamwise Vorticity

The vorticity vector Ω is defined as the curl of the velocity vector $\mathbf{q}$

$$\Omega = \nabla \times \mathbf{q}$$

A Cartesian coordinate system is set up as x, y, z in the axial, tangential (or pitchwise), and radial (or spanwise) directions, with velocity components u, v, and w, respectively. Thus the components of vorticity are

$$\Omega_x = \frac{\partial w}{\partial y} - \frac{\partial v}{\partial z}$$

$$\Omega_y = \frac{\partial u}{\partial z} - \frac{\partial w}{\partial x}$$

$$\Omega_z = \frac{\partial v}{\partial x} - \frac{\partial u}{\partial y} \tag{1}$$

In secondary flow theory, the streamwise vorticity is taken as the component of vorticity in the primary flow direction rather than the component in the local flow direction. Thus the streamwise vorticity may be taken as

$$\Omega_s = \Omega_x \cos \alpha_p + \Omega_y \sin \alpha_p \tag{2}$$

where α_p is the primary flow angle. It may be noted that the radial component Ω_z has no effect, since in a linear cascade the primary flow has no radial component by definition.

Estimation of the gradients $\partial/\partial z$ and $\partial/\partial y$ in the radial and tangential directions can be made from the data on a given transverse plane, because the spacing of data points is fairly close on each traverse plane. The axial gradient $\partial/\partial x$ is more difficult since the axial spacing is too large to allow reasonable direct estimation. An alternative is to use the incompressible Helmholtz equation

$$\mathbf{q} \times \Omega = \frac{1}{\rho} \nabla p_0 \text{ where } p_0 = \text{total pressure}$$

Taking the radial, or z, component

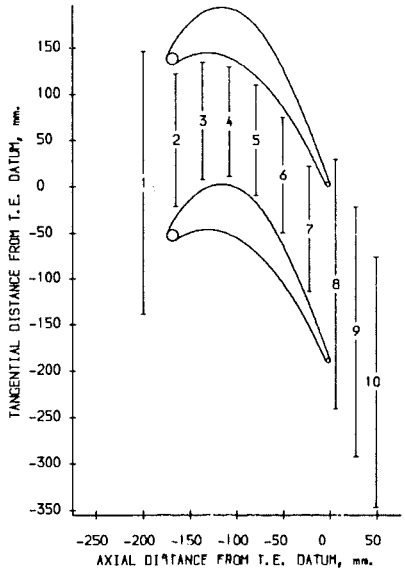

Fig. 1 Cascade design data

$$u\Omega_y - v\Omega_x = \frac{1}{\rho} \frac{\partial p_0}{\partial z}$$

Thus

$$\Omega_y = \frac{1}{u}\left[\frac{1}{\rho} \frac{\partial p_0}{\partial z} - v\Omega_x\right]$$

with Ω_x given from equation (1).

So the axial and tangential components of vorticity, required for the streamwise vorticity given by equation (2), may be found from the gradients of velocity and stagnation pressure on a given traverse plane. In this cascade, the flow at midspan was very little affected by the secondary flows on the endwalls. Thus the primary flow angle α_p in equation (2) was taken as the angle at midspan for the given tangential position. For traverse planes within the blade, the value of α_p varied considerably across the pitch, but downstream of the trailing edge α_p was fairly constant.

The differentiation of experimental data is notoriously difficult, since experimental scatter can cause unrealistic values of gradient. The approach used was to fit a least-square bicubic spline surface to the data points, and to take the gradient of the surface in the required direction at each data point coordinate. The tightness of fit of a spline is controlled by the number of interior knots, and the position and number of knots can only really be determined by inspection. With the large amounts of data, it was impractical to inspect each set, but some typical sets were inspected and the results applied generally. It was found that if the fit was made too close, the spline "wriggled" through the data. However too loose a fit would miss real characteristics of the data. The procedure finally adopted was to start with relatively few knots and compare the sum of the residuals with the variance of the data. The number of knots was progressively increased until the sum was sufficiently small. The criterion chosen was that the average residual had to be less than 5 percent of the variance. As the results show, this approach gave a reasonable picture of

Nomenclature

p_0 = total pressure
q = velocity vector
u = velocity component in x direction
v = velocity component in z direction
x = axial coordinate
y = tangential or pitchwise coordinate
z = radial or spanwise coordinate
α = flow angle in x–y plane
ρ = density
Ω = vorticity

the growth of streamwise vorticity through the cascade, although there are a few places where unlikely values appear.

The values of vorticity obtained were made dimensionless by using the upstream velocity and the blade chord. The choice of chord was somewhat arbitrary; other length scales such as pitch, span, or inlet boundary layer thickness could have been chosen.

Results

Surface Flow Visualization. Figures 2 and 3 show pictures of the flows on the endwall and suction surfaces. The surfaces were covered with thin plastic adhesive film before painting with the dye and oil mixture, and the film removed for photography. The pictures were taken using ultraviolet light, which improved the contrast due to the fluorescence of the pigment. Figure 2 shows the complicated flow pattern on the endwall, with the blade profile appearing somewhat unclear due to the ragged edges of the plastic film. Most clearly shown is the cross-passage separation line between the blades due to the pressure side leg of the horseshoe vortex and the passage vortex. There are strong cross-passage flows on the downstream side of this separation that feed low-momentum fluid into the passage vortex. After meeting the suction surface the separation line follows the blade surface, but is displaced from it by a small distance. This is due to the presence of a countervortex in the suction surface and endwall corner. The picture is similar to that reported by other workers, e.g., Langston et al. (1977) and Marchal and Sieverding (1977), although the visualization did not extend sufficiently far upstream to detect the saddle point near the leading edge.

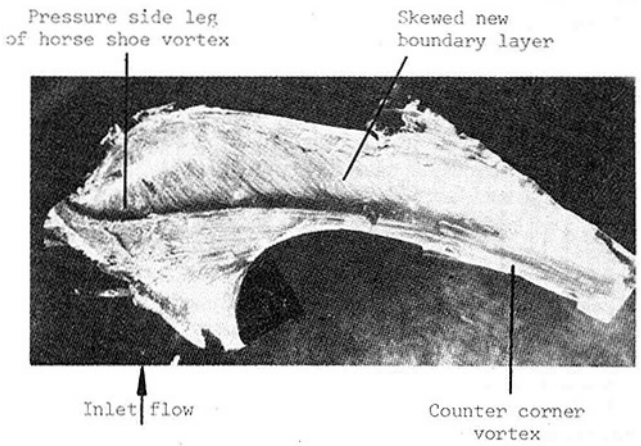

Fig. 2 Endwall flow

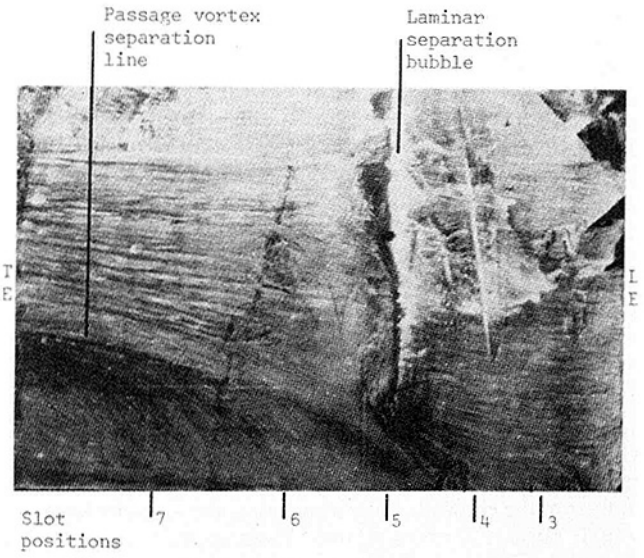

Fig. 3 Suction surface flow

In Fig. 3, which is a developed view of the suction surface, a laminar separation bubble is clearly seen extending some 75 percent of the spanwise distance from midspan to the endwall. The separation line due to the suction surface leg of the horseshoe vortex may be seen moving up the suction surface and disappearing into the separation bubble. This is different from that observed by other workers who used a boundary layer trip to avoid the separation bubble, e.g., Marchal and Sieverding (1977). The separation line due to the passage vortex is seen to move up the suction surface as the vortex grows in size, and there is evidence of strong spanwise flows away from the endwall. Also indicated on Fig. 3 are the slot traverse positions in the second half of the blade passage; these will be referred to in the next section.

Area Plots. In Fig. 4 onward a selection of results are presented as area plots at a number of the traverse planes within the passage. The contours of vorticity and total pressure loss and the secondary velocity vectors are placed alongside each other for easy comparison. The vertical axis is the spanwise distance from the endwall. The horizontal axis is the pitchwise distance measured from a trailing edge datum and positive going from suction to pressure surface. Thus the suction surface appears on the left and the pressure surface on the right.

In Fig. 4, at slot 3 (22 percent of axial chord from the leading edge), the passage vortex has started to form, as shown by the negative vorticity near the endwall and by the velocity vectors. There is a small amount of positive vorticity near the suction surface corner, which may arise from the suction side leg of the horseshoe vortex as it reaches the suction surface. The total pressure contours are beginning to roll up under the action of the passage vortex. By slot 5, Fig. 5, the passage vortex has intensified, with high values of negative

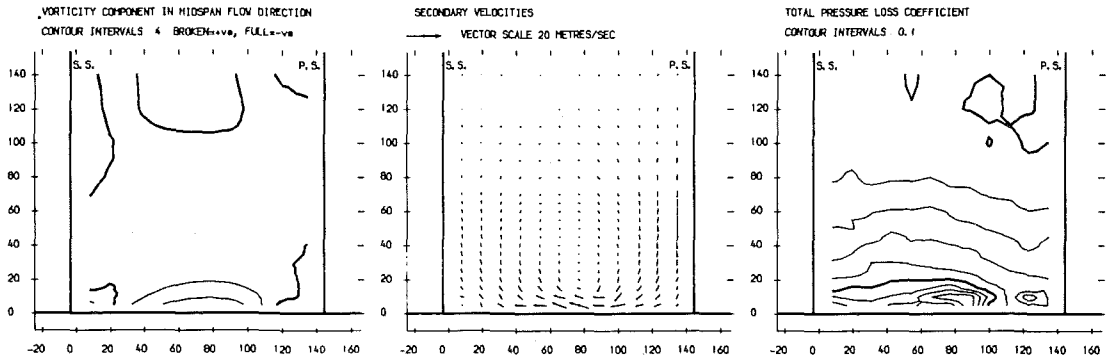

Fig. 4 Slot 3 natural inlet boundary layer

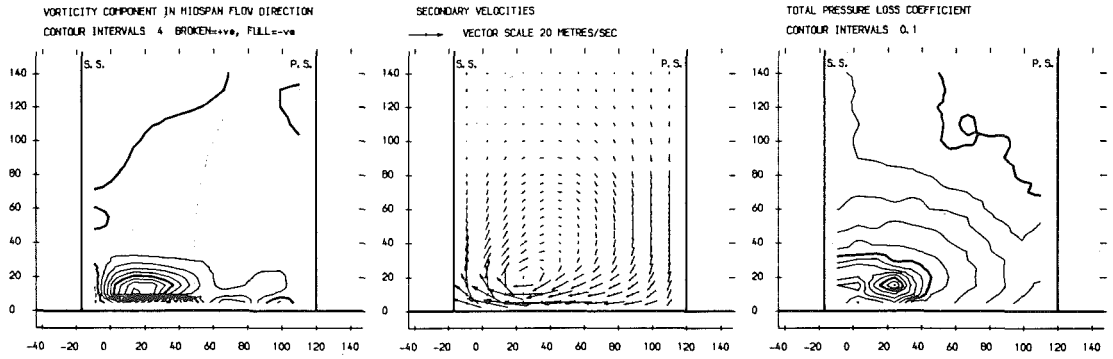

Fig. 5 Slot 5 natural inlet boundary layer

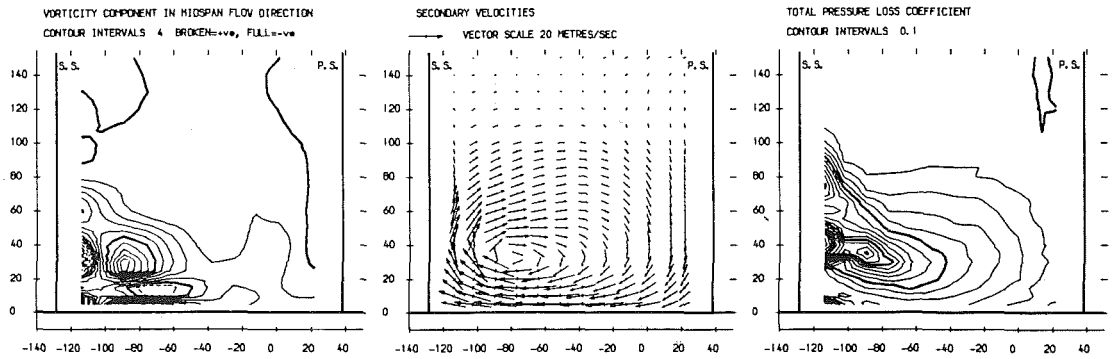

Fig. 6 Slot 7 natural inlet boundary layer

vorticity, and the vortex center has moved closer to the suction surface. There is a small area of positive vorticity in the suction surface corner, as the countervortex starts to grow. It extends some 20 mm up the suction surface to the position where the flow visualization in Fig. 3 would indicate the presence of the passage vortex separation line. However this description must be tentative because another thin area of positive vorticity is seen close to the end wall from about 10 mm to 50 mm tangential position. This may be due to the separation line on the end wall which Fig. 2 shows to be about 25 mm from the suction surface, i.e., at a tangential coordinate of 10 mm. A separation line will lead to an area of positive vorticity, but the tangential extent of this area on the endwall seems too great. It may be that the positive vorticity arises, at least in part, from poor surface fitting at the edge of the map of data points. The rolling up of the total pressure contours is quite severe with the clear formation of a loss core. There is a small region of higher loss near the suction surface at about 15 mm from the end wall. This is probably due to loss from the blade surface being fed into the bulk flow by the passage vortex separation line.

At slot 7, Fig. 6, near the trailing edge, the passage vortex dominates the scene with a large peak of negative vorticity. The secondary velocities are quite large, up to about 25 m/s compared with the exit midspan velocity of 35 m/s. Within the region of the passage vortex is enclosed a region of small positive vorticity. This is most likely due to the problems of surface fitting where there are adjacent very high values of negative vorticity. The positive vorticity in the corner vortex is quite clear, but it is now separated from a larger positive region centered at about 35 mm from the endwall. There is also a high loss peak close to the suction surface at about 40 mm from the endwall. The flow visualization in Fig. 3 shows the passage vortex separation line to be about 70 mm from the endwall at slot 7. So the region of high loss and positive vorticity is about halfway up the suction surface to the separation line. At 60 mm from the endwall, there is a peak in negative

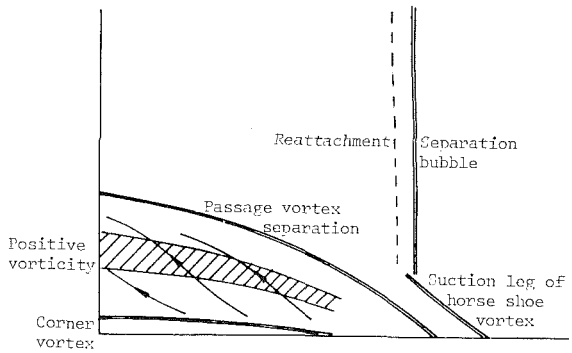

Fig. 7 Suction surface flow features

vorticity, which corresponds to the clear region on the flow visualization picture below the separation line. This line corresponds to the smaller loss peak on the suction surface at 75 mm from the endwall, while above this, the vorticity becomes weakly positive at about 90 mm. These same features are also seen at slot 6 (not shown here) with the high positive vorticity and loss peak close to the suction surface at 25 mm from the end wall, the negative peak of vorticity at 40 mm, and the separation line and smaller loss peak at 45 mm.

While it can easily be understood that a separation line must involve two areas of vorticity with opposite sign, the large positive patch of vorticity and associated loss peak, seen about halfway up the suction surface to the vortex separation line, does not correspond to any separation line on the surface flow visualization, either here or reported elsewhere. Nor is the positive vorticity clear from visual inspection of the secondary flow vectors. The clear area just below the separation line may be explained by the high negative vorticity producing a scouring action close to the blade surface. Below the clear area, the surface flow lines form an S shape, as shown in the sketch of Fig. 7. Although this is not very clear from the photograph of Fig. 3, it is shown by other photographs, and has also been

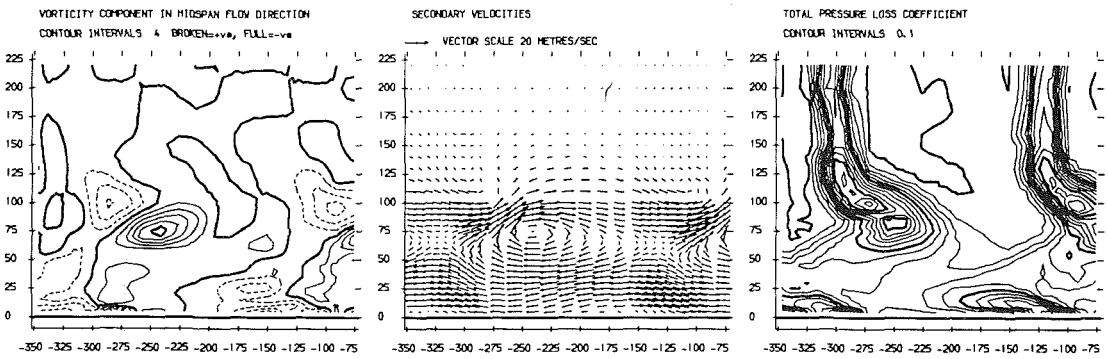

Fig. 8 Slot 10 natural inlet boundary layer

observed by other authors (e.g., Langston et al., 1977). It appears that the curving back away from the spanwise direction caused by positive vorticity is also accompanied by an accumulation of loss brought up from the blade surface. This would explain the shape of the downstream loss core picture, with relatively low loss below the core (see Fig. 8).

Figure 8 (slot 10) also shows the shed vorticity, which is positive, in the blade wakes. In classical theory terms this corresponds to the trailing filament and trailing shed vorticity. By slot 10 the wake is distorted by the under and overturning crossflows as seen in the vector plots. The results at slot 8 (not shown) just downstream of the trailing edge show the shed vorticity contained in a near-vertical wake. The shed vorticity has separated into two distinct areas. The lower one near the wall is linked with the corner vortex seen at slot 7, Fig. 6, but it contains more positive vorticity than in the corner vortex alone. The upper area seen at about 100 mm from the endwall contains the positive patch of vorticity discussed above, although convected away from the endwall by the passage vortex. The peak value of negative vorticity in the passage vortex is lower than at slot 7, due to viscous dissipation as the flow proceeds downstream. Near midspan the streamwise vorticity is close to zero, as expected, giving some confidence in the method of obtaining vorticity by surface fitting. The loss at midspan shows the two-dimensional blade wakes, with a fair level of repeatability, which was achieved by increasing the number of data points there. The blade wake runs into the loss core, with a double loss peak. Near the endwall, the loss associated with corner vortex may be seen to be located in the same region as the positive vorticity, i.e., near the endwall at about -200 mm to -100 mm tangential position.

It may be noticed that in the figures showing the vorticity the only evidence of the suction side leg of the horseshoe vortex (which gives positive vorticity) is at slot 3 close to the suction surface and endwall corner. The flow visualization in Fig. 3 shows the separation line joining the laminar separation bubble and then disappearing. Moore (1983) has shown that fluid from the suction side leg of the horseshoe vortex is convected around the outside of the passage vortex away from the suction surface. However his cascade was of lower aspect ratio so that the passage vortices from the two endwalls interacted strongly, and also the blades had a boundary layer trip. It may be that the difference in the two cascades has a large effect on the flow, but in this work no evidence is seen of the vorticity due to the suction side leg of the horseshoe vortex being convected away from the suction surface.

Pitch-Averaged Results. The data were averaged across the pitch, taking a mass mean where appropriate, e.g., for loss and crossflow velocities. Presented here is a selection of the results for yaw angle, total pressure loss coefficient and the kinetic energy of the secondary velocities (made dimensionless with respect to inlet mainstream velocity), and the streamwise vorticity.

Results for slots 3, 5, 7, and 10 are shown in Fig. 9. At slot 3 there is small overturning of 10 deg with a corresponding generation of weak negative vorticity, the mean mainstream turning being from the nominal inlet angle of 42.75 deg to about 19 deg. The loss is similar to that shown at slot 1, just upstream of the cascade, with a small generation of secondary kinetic energy. At slot 5, the profiles of overturning and vorticity are similar to those at slot 3, but of a greater magnitude. The positive vorticity point near the endwall should probably be ignored as it is caused by the patch seen in Fig. 5 and discussed earlier. However, the secondary kinetic energy is now quite large near the wall and the loss profile shows the effect of the rolling up of the Bernoulli surfaces to form the loss core. Up to slot 5, the streamwise vorticity and yaw angle appear similar to what would be expected from secondary flow theory. However beyond slot 5, e.g., at slot 7, the distortion of the Bernoulli surfaces greatly affects the streamwise vorticity generation, which gives an uneven profile caused by the patches of positive vorticity seen in Fig. 6. The peak intensity is less, as is the magnitude of overturning, with some underturning becoming apparent. The peak secondary kinetic energy is also reduced, and the loss peak is farther away from the wall. At the downstream slot 10, the shed vorticity in the blade wakes causes two regions of pitch-averaged positive vorticity, separated by a region of negative vorticity. The yaw angle shows a sharp underturning at slot 10, and the overturning near the endwall is reduced by the effects of the corner countervortex. The secondary kinetic energy shows two peaks, corresponding to the positions of maximum overturning and underturning. The loss core peak has been convected away from the endwall, reduced in magnitude, and broadened compared with slot 7. A second peak is seen near the endwall due to the loss from the corner vortex, and at midspan the profile loss is apparent.

Effect of Inlet Boundary Layer Thickness. The flows at the downstream traverse plane, slot 10, with the thick and thin inlet boundary layer are shown in Figs. 10 and 11. These may be compared with Fig. 8 for the natural inlet boundary layer. The positions of the main features of the flow are very similar with the loss core, endwall loss region, and apparent vortex center being at nearly the same coordinate values. The main difference seems to be that as the inlet boundary layer is thickened, the features become broader and less intense. This is particularly true for the vorticity. Figure 10 shows that both the positive and negative vorticity peak values are much lower than in Fig. 11. This may be understood in terms of the inlet normal vorticity to the cascade; the thinner boundary layer will have higher vorticity values that are more concentrated near the endwall. However secondary flow theory would not predict the convection of the vorticity away from the endwall

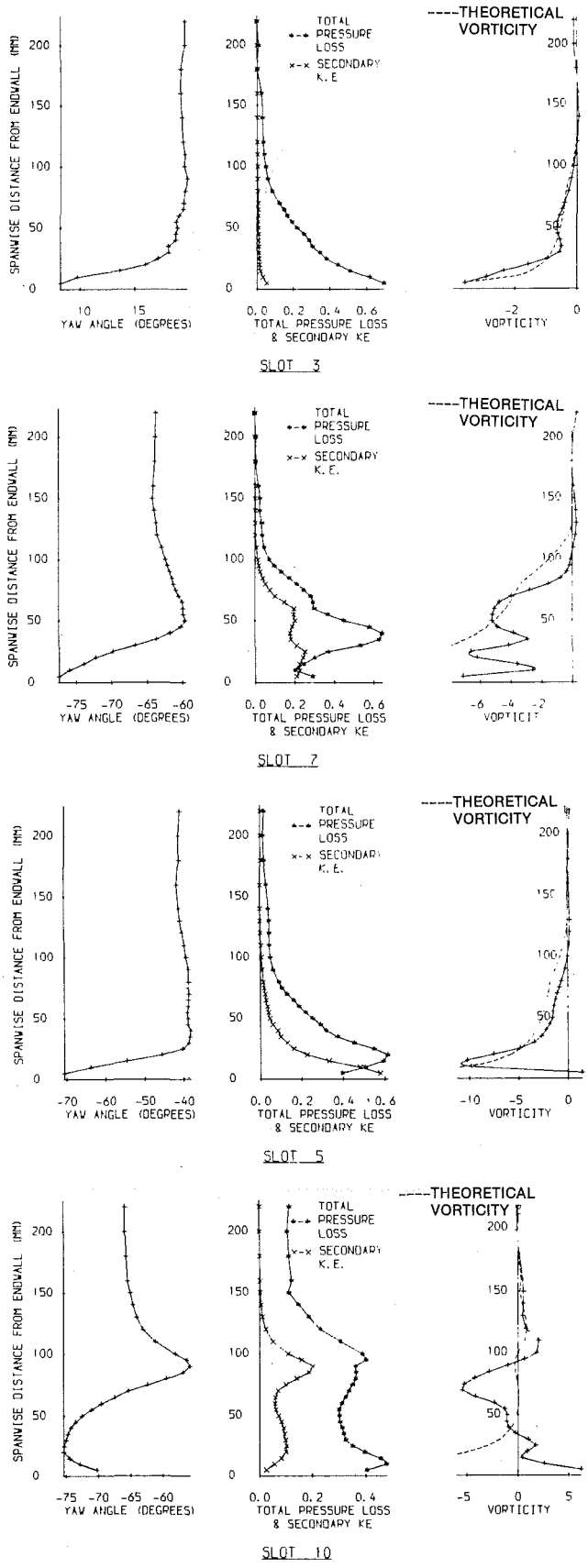

Fig. 9 Pitch-averaged results

so that the passage vortex is similarly placed irrespective of boundary layer thickness. It should be noted that even for the thin boundary layer, the ratio of thickness to blade pitch is quite large (0.43) compared to most other workers (see Sieverding, 1985).

Table 3

Boundary layer type	Natural	Thick	Thin
Slot 10 mixed-out loss coefficient	0.294	0.413	0.298
Mixed-out profile loss	0.103	0.106	0.116
Gross secondary loss	0.191	0.307	0.182
Inlet loss	0.084	0.175	0.054
Net secondary loss	0.107	0.132	0.128

Area-Averaged Results. The growth of loss, secondary kinetic energy, and streamwise vorticity are shown in Fig. 12. The quantity concerned was mass meaned over the traverse plane for each slot, the positions of which are indicated underneath the loss curve. Upstream and downstream, the averaging was done over one pitch width, whereas the data were taken over about 1.5 pitch. The error bands shown were obtained by varying the tangential position of the pitch distance for the averaging. Some caution should be exercised for slots 8 and 9, because the data points were not sufficiently close within the blade wakes to give good definition. This explains the large error band on the loss for slot 8 and why the loss falls from slot 8 to 10. The dotted line shows a more reasonable trend, the point at lot 8 being estimated from slot 7 plus an allowance for the additional profile loss. Although the loss is suspect at slots 8 and 9, the vorticity and secondary kinetic energy seem reasonable.

The vorticity and secondary kinetic energy grow steadily through the cascade (apart from the vorticity at slot 4, which seems high). After the trailing edge the vorticity drops suddenly due to the addition of the shed vorticity in the blade wakes. The secondary kinetic energy starts to decay slowly after the trailing edge. It may be noted that this is in contrast to Moore and Adhye's (1985) results, where both the level of kinetic energy and its rate of decay were much higher. The difference may be due to the lower aspect ratio of their cascade, with interaction of the two passage vortices, such that the whole flow is dominated by secondary effect. The loss also grows steadily although it appears to increase more rapidly toward the trailing edge as loss from the blade suction surface is fed into the bulk flow. It should be noted that the traverse did not go close enough to the blades or endwall to pick up the thin boundary layers, so these results represent what is happening to the bulk flow, rather than giving the true total loss at each plane.

At the downstream plane, slot 10, the mixed-out loss values were calculated, from which the total net secondary loss may be estimated. These are shown in Table 3 along with the results for the thick and thin inlet boundary layers.

The use of mixed-out loss rather than the actual loss at the traverse plane should remove the dependence of the loss on the downstream traverse plane position, at least to some extent. There will be an increase due to shearing on the endwall, but this is likely to be small compared with the loss growth through the cascade. Table 3 shows no clear trend of net secondary loss with inlet boundary layer thickness, and this has been found by other workers, e.g., Atkins (1985).

Theoretical Comparison

The classical secondary flow theory was applied to the cascade. At exit, it was not expected to give good comparisons with experiments because of the distortion of the Bernoulli surfaces, clearly seen in the experiments. However a comparison may be made within the blade passage, at least on a pitch-averaged basis for secondary vorticity. The theoretical

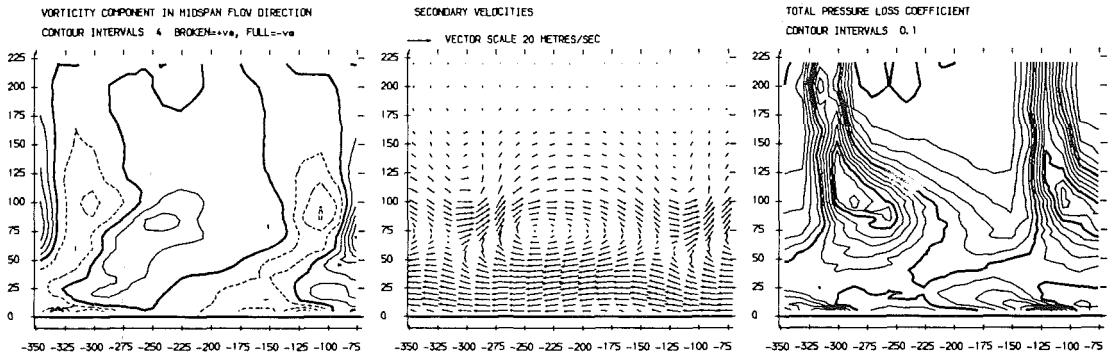

Fig. 10 Slot 10 thick inlet boundary layer

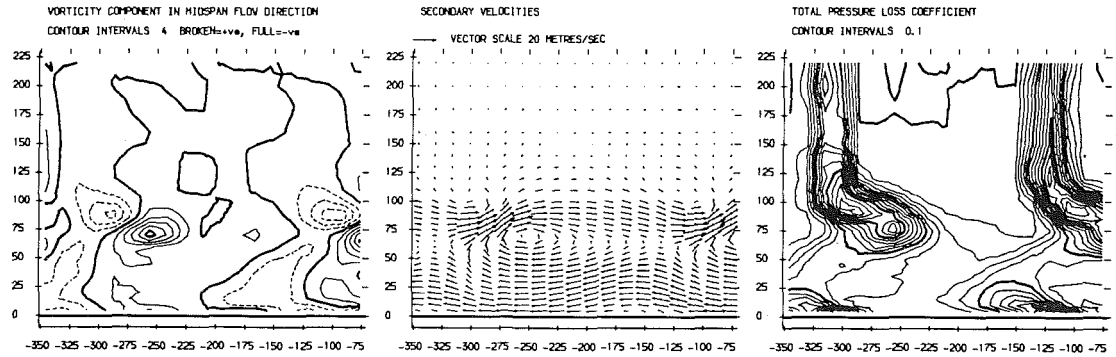

Fig. 11 Slot 10 thin inlet boundary layer

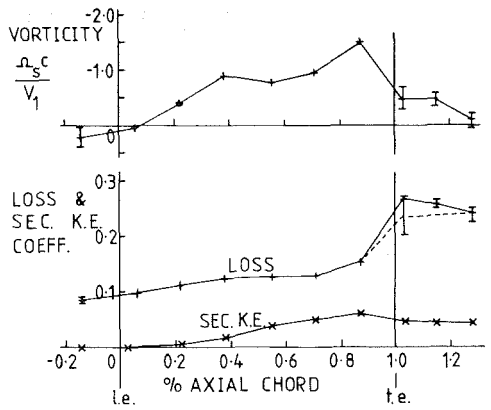

Fig. 12 Area-averaged loss, secondary kinetic energy, and vorticity

prediction was made by using the Came and Marsh (1974) formula taking the turning angle from the pitch-averaged yaw angle at the slot traverse position concerned. Figure 9 also shows the theoretical results for slots 3, 5, 7, and 10. For slot 10, the theoretical prediction includes the blade shed vorticity components. The theoretical prediction derived the inlet normal vorticity from a power low inlet boundary layer profile of thickness 102 mm and exponent 0.149. Since a power low profile gives a discontinuity in slope at the boundary layer edge, some smoothing was done between 80 mm and 120 mm.

At slot 3, the agreement is very good, but by slot 5, the vorticity is predicted too high beyond 25 mm. At slot 7, the vorticity is predicted much too high near the end wall, while at slot 10, the prediction seems to bear little relation to the experiment. There seems to be a progressive deterioration beyond slot 5, which accords with the observation of the rolling up of the total pressure contours from slot 5 onward. The action of the secondary flows produces this distortion, and also produces a convection of itself away from the endwall. There is no mechanism for this in the theory. Thus at slot 7 the agreement away from the endwall is probably rather fortuitous; the overprediction of vorticity due to not taking the Bernoulli surface twisting into account has been balanced by the outward convection of vorticity by the secondary flows. At slot 10, this outward convection is clear with the negative peak at around 70 mm from the wall. In addition the effects of viscosity are evident close to the wall, with the positive vorticity arising from a combination of the corner vortex and shed vorticity.

The above observations suggest that some modification to the theoretical method might be made to account for the Bernoulli surface distortion and the outward convection of vorticity. Glynn (1982) produced a method for tracing the Bernoulli surfaces through the cascade giving a loss core due to the rolling up of the surfaces. Work currently in progress at Durham University is investigating this approach further with the aim of producing a simple and fast estimation for secondary flows without the need for a fully three-dimensional calculation method.

Conclusions

1 The development of secondary flows and losses through a cascade of high turning rotor blades has been studied. Of particular interest is the presentation of the development of streamwise vorticity. To obtain this was not straightforward, but required the differentiation of experimental data using surface fits. Apart from one or two places, the results seem to be reasonable.

2 The development of the flow has been related to surface flow visualization, particularly with respect to the separation lines caused by the passage vortex and the two legs of the horseshoe vortex.

3 The development of the negative streamwise vorticity related to the passage vortex has been illustrated. Areas of positive vorticity are seen to be associated with separation lines and the feeding of loss into the mainstream. The main

positive area in the latter part of the passage lies about halfway between the endwall and the separation line on the suction surface caused by the passage vortex. This is associated with a significant feeding of loss into the bulk flow from the lower part of the suction surface.

4 The suction side leg of the horseshoe vortex is only seen in the early part of the passage. It appears either to be dissipated or absorbed into a separation bubble on the suction surface toward midspan. The pressure side leg merges with the passage vortex, which has the same sense of vorticity.

5 The streamwise vorticity predicted by secondary flow theory agrees well with observation in the first half of the passage. However in the second half, the progressive distortion of the Bernoulli surfaces and the outward convection of the passage vortex cause a deterioration in the validity of the theoretical prediction. The theory predicts that downstream of the blades, the magnitude of streamwise vorticity will drop due to the addition of the trailing shed and trailing filament vorticity in the blade wakes. A drop is observed, but the distribution of vorticity downstream is very different from that predicted. In addition viscous effects are seen to modify the vorticity, particularly close to the endwall.

6 Development of the theoretical method is suggested to include the effects of convection and Bernoulli surface distortion.

7 The effect of inlet boundary layer thickness is seen to affect the intensity of the secondary flow features, but with little change to their location.

Acknowledgments

This work has been carried out with the support of the Procurement Executive of the Ministry of Defence. The authors also gratefully acknowledge additional support from Rolls-Royce plc and permission to publish this paper. The authors also thank M. Howard for his contribution to the derivation of streamwise vorticity.

References

Atkins, M. J., 1985, "End Wall Profiling in Axial Flow Turbines," Ph.D. Thesis, Cambridge University, United Kingdom.

Came, P. M., and Marsh, H., 1974, "Secondary Flow in Cascades: Two Simple Derivations for the Components of Vorticity," *Journal Mechanical Engineering Sciences*, Vol. 16, pp. 391–401.

Glynn, D. R., 1982, "Calculation of Secondary Flow in Cascades Including Effects of Bernoulli Surface Distortion," *International Journal of Heat and Fluid Flow*, Vol. 3, pp. 73–80.

Graves, C. P., 1985, "Secondary Flows and Losses in Gas Turbines," Ph.D. Thesis, Durham University, United Kingdom.

Gregory-Smith, D. G., and Graves, C. P., 1983, "Secondary Flows and Losses in a Turbine Cascade," in: *Viscous Effects in Turbomachines*, AGARD CP 351.

Hawthorne, W. R., 1951, "Secondary Circulation in Fluid Flow," *Proceedings Royal Society*, Series A, Vol. 206, pp. 374–387.

Hawthorne, W. R., 1967, "The Applicability of Secondary Flow Analysis to the Solution of Internal Flow Problems," in: *Fluid Mechanics of Internal Flow*, G. Sovran, ed., Elsevier, New York, pp. 238–269.

Horlock, J. H., and Lakshminarayana, B., 1973, "Secondary Flows: Theory, Experiments and Applications in Turbomachinery Aerodynamics," *Annual Review of Fluid Mechanics*, Vol. 5, pp. 247–280.

Langston, L. S., Nice, M. L., and Hooper, R. M., 1977, "Three-Dimensional Flows Within a Turbine Cascade Passage," ASME *Journal of Engineering for Power*, Vol. 99, pp. 21–28.

Marchal, P., and Sieverding, C. H., 1977, "Secondary Flows Within Turbomachinery Blading," in: *Secondary Flows in Turbomachines*, AGARD CP 214.

Moore, J., 1983, "Flow Trajectories, Mixing and Entropy Fluxes in a Turbine Cascade," in: *Viscous Effects in Turbomachines*, AGARD CP 351.

Moore, J., and Adhye, R. Y., 1985, "Secondary Flows and Losses Downstream of a Turbine Cascade," ASME *Journal of Engineering for Gas Turbines and Power*, Vol. 107, pp. 961–969.

Sieverding, C. H., 1985, "Recent Progress in the Understanding of Basic Aspects of Secondary Flows in Turbine Blade Passages," ASME *Journal of Engineering for Power*, Vol. 107, pp. 248–257.

Squire, H. B., and Winter, K. G., 1951, "The Secondary Flow in a Cascade of Airfoils in a Non-uniform Stream," *Journal of Aeronautical Sciences*, Vol. 18, pp. 271–277.